Published in final edited form as:
Mol Imaging Biol. 2014 February ; 16(1): 85–94. doi:10.1007/s11307-013-0665-4.

Antagonistic Effects of Anti-EMMPRIN Antibody When Combined with Chemotherapy Against Hypovascular Pancreatic Cancers

Hyunki Kim[1,2,6,10], **Christopher J. Rigell**[3], **Guihua Zhai**[1], **S. Kyle Lee**[3], **Sharon L. Samuel**[1], **Amber Martin**[1], **Heidi R. Umphrey**[1,6], **Cecil R. Stockard**[6], **T. Mark Beasley**[4], **Donald J. Buchsbaum**[5], **Long Shan Li**[7,8,9], **David A. Boothman**[7,8,9], and **Kurt R. Zinn**[1,3,6]

[1]Department of Radiology, University of Alabama at Birmingham, Birmingham, AL, 35294-0019, USA

[2]Department of Biomedical Engineering, University of Alabama at Birmingham, Birmingham, AL, 35294-0019, USA

[3]Department of Medicine, University of Alabama at Birmingham, Birmingham, AL, 35294-0019, USA

[4]Department of Biostatistics, University of Alabama at Birmingham, Birmingham, AL, 35294-0019, USA

[5]Department of Radiation Oncology, University of Alabama at Birmingham, Birmingham, AL, 35294-0019, USA

[6]Comprehensive Cancer Center, University of Alabama at Birmingham, Birmingham, AL, 35294-0019, USA

[7]Department of Pharmacology, University of Texas Southwestern Medical Center, Dallas, TX, 75390-8807, USA

[8]Department of Radiation Oncology, University of Texas Southwestern Medical Center, Dallas, TX, 75390-8807, USA

[9]Simmons Comprehensive Cancer Center, University of Texas Southwestern Medical Center, Dallas, TX, 75390-8807, USA

[10]VH G082, 1720 2nd Avenue South, Birmingham, AL, 35294-0019, USA

Abstract

Purpose—To examine the antagonistic effects of anti-extracellular matrix metalloprotease inducer (anti-EMMPRIN) antibody when combined with chemotherapy using a hypovascular pancreatic tumor model.

Correspondence to: Hyunki Kim; Hyunki@uab.edu.

Conflict of Interest. Dr. Boothman is a consultant for StemPAR Sciences, Inc.

Procedures—Severely compromised immunodeficient mice bearing orthotopic MIA PaCa-2 tumors were used (five to six animals per group). Dynamic contrast-enhanced magnetic resonance imaging was used to examine the relationship between tumor vascularity and size. Therapy was initiated when tumors were hypovascular. Treatments included: (1) gemcitabine alone, (2) anti-EMMPRIN antibody alone, and (3) combination, each for 2 weeks. Additionally, another treatment arm included β-lapachone, an NAD(P)H/quinone 1 (NQO1) bioactivated agent. ^{18}F-fluoro-D-glucose-positron emission tomography/computed tomography imaging was used weekly to monitor therapeutic effects.

Results—Gemcitabine or anti-EMMPRIN monotherapy significantly delayed tumor growth, but the combination therapy showed an antagonistic effect. Similarly, tumor growth was significantly suppressed by β-lapachone alone, and additive effects were noted when combined with gemcitabine, but the therapeutic efficacy was reduced when anti-EMMPRIN antibody was added.

Conclusions—Anti-EMMPRIN antibody with chemotherapy in hypovascular tumors results in antagonistic effects.

Keywords

Pancreatic cancer; EMMPRIN; β-Lapachone; Gemcitabine; DCE-MRI; FDG-PET/CT

Introduction

Among all cancers affecting humans, pancreatic cancers are the most deadly. Pancreatic cancers are currently the fourth leading cause of cancer deaths in the United States but predicted to be the second leading cause of cancer death by year 2020. Gemcitabine, a nucleoside chain terminator, is the current standard of care for advanced pancreatic cancer, but it offers only minimal survival benefit for patients [1]. Gemcitabine is a prodrug requiring phosphorylation for DNA incorporation, thereby interfering only with cycling cancer cells resulting in apoptosis and senescence. Since gemcitabine functions in an S-phase-dependent manner, the therapeutic effect is limited to dividing cells and mostly leading to transient tumor growth suppression.

In contrast, β-lapachone is capable of killing tumor cells independent of cell cycle position and is specific for cancer cells expressing the two-electron oxidoreductase NAD(P)H/quinone oxidoreductase-1 (NQO1) [2, 3]. In the presence of NQO1, β-lapachone leads to robust formation of reactive oxygen species and Ca^{2+} release from endoplasmic reticulum stores. This results in the hyperactivation of poly (ADP-ribose) polymerase 1 (PARP1) that stimulates NAD+/ATP loss and programmed necrosis (necroptosis) [2–4]. β-Lapachone also acts as a potent inhibitor of DNA repair [5], suggesting a possible synergism with DNA damaging agents like gemcitabine.

Extracellular matrix metalloprotease inducer (EMMPRIN) is a glycoprotein expressed within the cellular membrane and is considered a promising target for efficacious therapy of pancreatic cancers [6]. EMMPRIN promotes matrix-metalloproteinase (MMP)-1, MMP-2, and MMP-3 production [7–9]; these MMPs function to degrade extracellular matrix components, resulting in tumor-cell invasion and metastasis [10]. EMMPRIN also promotes

tumor neovascularization by upregulating vascular endothelial growth factor (VEGF) isoforms and the VEGF receptor, VEGFR-2, via stimulation of hypoxia-inducible factor-1 alpha (HIF-1α) [11]. Therefore, an anti-EMMPRIN therapy may suppress tumor vascularization as well as metastasis.

The potential anti-vascularization effects of an anti-EMMPRIN therapy on pancreatic cancers suggest that great care must be taken when combination therapies with small-molecule chemotherapeutic agents such as gemcitabine or β-lapachone are applied. Fig. 1 illustrates the delivery of a non-targeting small-molecule (NTSM) chemotherapeutic agent over time to tumors with different vascularities. Hypervascular tumors contain dilated, tortuous and leaky vessels, causing high interstitial pressures [12]. The leaky vessels result in a high wash-in rate of the NTSM drug, but the corresponding washout rates are also high due to the high interstitial pressures. As a result, steady-state drug concentration (DC_{ss}) remains relatively low. However, isovascular tumors contain vessels with medium leakiness, so both penetrating drug levels and washout rates become modest, driving elevated DC_{ss} values. For hypovascular tumors, DC_{ss} values remain low since tumor vessels are relatively scarce. If an anti-EMMPRIN therapy is used for hypervascular tumors, its antiangiogenic effects may induce vascular normalization, reducing interstitial pressures [12]. Thus, the anti-EMMPRIN therapy may simultaneously reduce wash-in and washout rates and thereby improve drug-delivery efficiency and combination therapy efficacy. In contrast, for both isovascular and hypovascular tumors, the antiangiogenic effects of the anti-EMMPRIN therapy may cause significantly diminished drug delivery efficiency, inducing tumor hypoxia. The goal of this study was to determine the effects of an anti-EMMPRIN antibody therapy on two current chemotherapeutic agents being used for the treatment of pancreatic cancer, one standard of care agent (*i.e.*, gemcitabine) and another experimental agent, β-lapachone, in hypovascular pancreatic tumors.

Dynamic contrast-enhanced magnetic resonance imaging (DCE-MRI) was employed to analyze tumor vascularity non-invasively. DCE-MRI biomarkers, K^{trans} (forward volume transfer constant) and k_{ep} (reverse reflux rate constant), represent the wash-in and washout rates of an MR contrast, respectively [13]. 2-Deoxy-2-[^{18}F]fluoro-D-glucose (^{18}F-FDG) positron emission tomography (PET) and X-ray computed tomography (CT) imaging were employed to measure tumor-cell glycolysis and tumor volume, respectively [14–16].

Materials and Methods

Reagents and Cell Lines

All reagents were from Fisher (Pittsburg, PA), unless otherwise specified. Dr. Tong Zhou (UAB, Birmingham, AL) generously provided the purified monomeric monoclonal anti-EMMPRIN antibody (mouse origin IgG1 kappa). ^{18}F-FDG was purchased from PETNET Solutions (Birmingham, AL). MIA PaCa-2 human pancreatic cancer cells were obtained from Dr. Donald J. Buchsbaum (UAB, Birmingham, AL). It was cultured in Dulbecco's modified Eagle's medium (Mediatech Inc, Herndon, VA) supplemented with 10 % fetal bovine serum (Hyclone, Logan, UT). OmnipaqueTM (iohexol, 350 mg/ml, GE Healthcare Inc., Princeton, NJ), ProHance® (gadoteridol, an MR contrast agent; Bracco Diagnostics Inc., Princeton, NJ), and Gemzar (gemcitabine, Eli Lilly, Indianapolis, IN) were purchased

from the University of Alabama at Birmingham Hospital Pharmacy. We made β-lapachone and hydroxypropyl-β-cyclodextran (HPβ-CD, vehicle of β-lapachone) as previously described [2, 3].

Animal Modeling

Animal experiments were reviewed and approved by the Institutional Animal Care and Use Committee at UAB. Nine groups of female severely compromised immunodeficient BALB/c mice (NCI-Frederick Animal Production Program, Fredrick, MD, 4~ 6 weeks old) were used. The procedure for intrapancreatic tumor implantation was as follows: A 1-cm incision was made in the left upper quadrant of the abdomen of anesthetized mice, and 2.5×10^6 MIA PaCa-2 cells were injected into the tail of the pancreas. The skin and peritoneum were closed in one layer with three interrupted 5–0 Prolene sutures. Group 1 was used to examine changes in tumor vascularity with respect to tumor size; when tumors were palpable, *in vivo* ultrasound imaging was applied to select six animals bearing tumors with matching size and shape among ten animals, and then a vascular access port (PennyPort, Access Technologies, Skokie, IL) was subcutaneously implanted to facilitate repeated intravenous injection of an MR contrast agent (gadoteridol), as previously described [13, 17]. Four days after port insertion, T2-weighted MRI and DCE-MRI were performed for all animals of group 1 every 24 h for 4 days. Tumor volumes and vascular parameters (K^{trans}, k_{ep}, and C_{20min}) were quantified. C_{20min} is the concentration of gadoteridol at 20 min after dosing. Groups 2–9 were used for various therapies as outlined below. Forty-eight animals bearing tumors with similar sizes and shapes determined by *in vivo* ultrasound imaging were selected from 60 animals. Therapy schedule was determined based on results found with group 1. Drug dosing started when tumors were small enough to be considered hypovascular but larger than 2 mm in diameter, so as not to be considered avascular [18]. Group 2 served as a control; three mice were untreated, and the other three mice were injected with HPβ-CD (20 mg/kg, intravascular (IV), days 4, 6, 8, 10, and 12), the vehicle for β-lapachone. Groups 3–5 were injected with gemcitabine (100 mg/kg, IP, days 4, 8, and 12), anti-EMMPRIN antibody (0.2 mg, IP, days 0, 3, 7, and 10), or the combination, respectively. Group 6 was injected with β-lapachone (20 mg/kg, IV, days 4, 6, 8, 10, and 12) solubilized in HPβ-CD. Groups 7–9 were treated with the same doses and time schedule applied for groups 3–5, respectively, but β-lapachone was added to each regimen, in the same scheduling as used for group 6. When gemcitabine and β-lapachone were given on the same day, β-lapachone was administered at 2 h after gemcitabine injection. A total of six mice were initially used per group, but one animal of group 3 and one animal of group 9 died at 7 and 8 days after therapy started, respectively. ^{18}F-FDG-PET/CT imaging was performed weekly (days 0, 7, and 14). Body weights were measured weekly. At the end of each therapy, tumor and blood (100–200 μl) were collected from each mouse, and Ki-67 staining was performed for all tumor tissues. Densities of white blood (WBC), red blood (RBC), and proliferating (Ki-67 expressing) cells were measured. All mice were anesthetized using isoflurane gas (1~2 %) during imaging.

MR Image Analysis

Small animal DCE-MRI and T2-weighted imaging were conducted using a Bruker BioSpec 9.4 T system (Bruker BioSpin Corp., Billerica, MA). Tumors were imaged using a

combination of a ^{1}H volume resonator/transmitter and a surface coil receiver (Bruker BioSpin Corp., Billerica, MA). A T2-weighted spin-echo sequence (RARE) was used with the following parameters—repetition time/echo time (TR/TE)=2,000/34 ms, 128×128 matrix, 1 mm thickness, and 30×30-mm field of view. Continuous 1-mm thick slices were used to cover the entire tumor region. A T1 map was acquired with a FLASH gradient-echo multiflip-angle approach with the following parameters—TR/TE=115/3 ms, 128×128 matrix, 1-mm thickness, 30×30-mm field of view, NEX=4, and seven flip angles of 10, 20, 30, 40, 50, 60, and 70°. A total of three to five 1-mm thick slices were acquired to cover tumor regions of interest in an interlaced mode. DCE-MRI employed the same acquisition parameters as those above but with a fixed flip angle of 30° and temporal resolution of 58.88 s. Five baseline images were acquired before gadoteridol injection, and then 20 images were acquired after gadoteridol injection of 0.0267 mmol/ml over a period of 15 s with a total injection volume of 0.15 ml. The reference region model was employed to calculate volume transfer constant (K^{trans}) and rate constant (k_{ep}), as described [13], but a moving average filter (window: 3) was applied for the signal curve 1 min after contrast injection to further improve signal-to-noise ratios. Tumor areas were segmented from anatomical MR images using signal-intensity differences between region of interest (ROI) and background, and 0.5-mm peripheral regions were determined as described [13]. K^{trans}, k_{ep}, and C_{20min} values were averaged in the 0.5-mm peripheral tumor region to reduce quantification error contributing from a necrotic core. Segmentation of whole tumor areas was performed using ImageJ, version 1.44p (National Institutes of Health, Bethesda, MD), while quantification of K^{trans}, k_{ep}, and C_{20min} values and segmentation of peripheral tumor regions were implemented using computer software developed with Labview 2010, version 10.0.1 (National Instruments Co., Austin, TX).

PET/CT Image Analysis

Positron emission tomography/computed tomography (PET/CT) imaging was conducted using Triumph, a PET/CT dual-modality imaging system (GE, Northridge, CA) as described [19]. Tumor areas were manually segmented from contrast-enhanced CT images based on the signal-intensity differences between ROI and background. Standardized uptake values (SUVs) were calculated by $SUV=(C\times W)/D$ where C was tissue activity concentration (megabecquerels per milliliter), W was animal body weight (gram), and D was administered dose (megabecquerels). The whole tumor segmentation and PET/CT image co-registration were implemented with ImageJ, version 1.44p (National Institutes of Health, Bethesda, MD), while SUVs were quantified using computer software developed with Labveiw 2010, version 10.0.1 (National Instruments Co., Austin, TX).

Ultrasound Image Analysis

Ultrasound imaging was performed using a VisualSonics VEVO 660 high-frequency, high-resolution ultrasound instrument with a 40 MHz probe (Toronto, Ontario, Canada) as described [20]. In the anterior–posterior plane, the largest diameter and the maximum diameters perpendicular to it were measured. Then the ultrasound probe was rotated 90° to measure the largest diameter in the sagittal plane. The tumor volume was calculated using the following, Volume = $xyz(\pi/6)$, where x, y, and z were the three orthogonal diameters of a tumor.

Histological Analysis

Ki67 staining was performed for tumor tissues of all mice with the same procedure as reported [21]. Two digital pictures (×200) were randomly taken in a blinded manner for each tumor slice using a SPOT camera on a Nikon Optiphot-2 microscope (Nikon inc., Melville, NY), interfaced with a personal computer and SPOT software. Proliferative (Ki67-expressing) cells were segmented by color differences, while the color threshold was manually determined. Cell densities were determined as the number of target cells per unit area. Image segmentation and cell counting were implemented using ImageJ, version 1.44p (National Institutes of Health, Bethesda, MD).

Statistical Analysis

One-way ANOVA was performed to compare initial tumor volumes, animal body weights, Ki-67-expressing cell densities, and blood-cell densities among groups 2–9 [22]. Two-way repeated-measures ANOVA was employed to compare tumor volume and SUV_{mean} changes over 2 weeks for groups 2–9 [23]. Pearson's correlation coefficient was computed to analyze linear relationships between the two variables [24]. Pearson's correlation coefficients were also obtained to correlate Ki-67-expressing cell densities and tumor volume changes (or tumor SUV_{mean} change). *P* values less than 0.05 were considered significant, while applying Bonferroni correction for multiple comparisons [22]. Data were presented as mean±standard error. All analyses were performed using SAS, version 9.2 (SAS Institute Inc., Cary, NC).

Results

MIA PaCa-2 Tumor Vascularity Correlated with Tumor Size

Fig. 2a shows gadoteridol concentration (millimolar) in three representative mice bearing orthotopic MIA PaCa-2 tumors with different sizes (80, 120, and 300 mm^3, respectively) at 0, 5, and 20 min post-contrast administration. Tumor region is indicated with a black circle in each sub-figure. Fig. 2b shows contrast-enhancement curves (dots) averaged in the ROIs indicated with white squares (2 pixels per square located in the peripheral tumor region) in the images at 0 min (Fig. 2a), together with best-fit fifth-order polynomial curves (dotted lines), while dosing time is indicated with a black arrow. The gadoteridol concentration in the large tumor (300 mm^3) was markedly higher than that in the midsize tumor (120 mm^3) during the early phase of injection but rapidly decreased over time. On the other hand, the contrast concentration in the midsize tumor was lower than that in the large tumor during the early phase. However, the gadoteridol concentration in the midsize tumor increased gradually and was maintained higher by about 10 min post-administration. For the small tumor, gadoteridol delivery was modest over the entire monitoring time due to its underdeveloped vascularity. Fig. 2c shows the second-order polynomial relationship between mean tumor volumes and mean K^{trans} values (R^2=0.99). The maximum K^{trans} value on the best-fit second-order polynomial curve is 0.071 min^{-1} at 263 mm^3. Similarly, Fig. 2d shows the second-order polynomial relationship between mean tumor volumes and mean k_{ep} values (R^2=0.99). The maximum k_{ep} value on the best-fit second-order polynomial curve is 0.107 min^{-1} at 217 mm^3. Fig. 2e shows averaged C_{20min} values according to the tumor size. C_{20min} was maximized when tumor volume was approximately 130 mm^3 but gradually decreased in larger tumors. Fig. 2f shows the relationship between mean C_{20min} and mean

K^{trans} values. C_{20min} was maximized when K^{trans} value was about 0.050 min^{-1} and then declined with larger values. Tumors with K^{trans} values lower than 0.05 min^{-1} were considered hypovascular for subsequent therapy. The mean tumor volume of groups 2–9 was 115±9 mm^3 prior to therapy initiation (day 0), so the average tumor K^{trans} value was estimated to be 0.045± 0.003 min^{-1} from the association between tumor volume and K^{trans} value shown in Fig. 2c.

Antagonistic Effect Between Anti-EMMPRIN Antibody and Chemotherapy

Fig. 3a shows representative ^{18}F-FDG PET/CT co-registered images of mice from groups 2–9 at 2 weeks after therapy initiation. Tumor location is indicated by a white circle in each sub-figure. Fig. 3b, f shows changes in tumor volumes and SUV_{mean} over 2 weeks after therapy, when animals were untreated (control) or treated with gemcitabine, anti-EMMPRIN antibody, or combination therapy, respectively. Gemcitabine or anti-EMMPRIN monotherapy delayed tumor growth significantly, but the combination did not improve therapeutic efficacy. Fig. 3c, g shows changes in tumor volumes and SUV_{mean} of control animals or groups treated with gemcitabine, β-lapachone, or combination, respectively. During the first 7 days post-treatment, additive effects were noted with either tumor volume changes (decreases of 53 % *versus* 42 %) or SUV_{mean} values (decreases of 40 % *versus* 39 %), and overall efficacy gradually decreased over the next 7 days. Fig. 3d, h shows changes in tumor volume and SUV_{mean} values of four groups untreated (control) or treated with β-lapachone, anti-EMMPRIN antibody, or combination, respectively. An antagonistic effect was noted when animals were treated with anti-EMMPRIN antibody and β-lapachone combination compared with either agent alone. Fig. 3e, i shows changes in tumor volumes and SUV_{mean} values for mice untreated (control) or treated with anti-EMMPRIN antibody, combination therapy with β-lapachone and gemcitabine, and the triple combination therapy, respectively. The antagonistic effect of anti-EMMPRIN antibody appeared more obvious when combined with two chemotherapeutic agents.

Histological Analysis

Fig. 4a shows representative microphotographs of Ki-67-stained tumor tissues of groups 2–9. Proliferative (Ki-67 expressing) cells are stained dark brown. Fig. 4b shows the proliferative cell densities (indicated with N/mm^2) of tumors of groups 2–9, but no statistical differences were found among these groups ($p>0.05$). Fig. 4c, d shows a linear relationship between mean proliferative cell densities and mean changes in tumor volumes (or SUV_{mean}) for 2 weeks post-treatment.

Toxicity Assessments

The body weights of mice treated as described above in groups 2–9 were not significantly altered post-treatment. The mean body weights of mice in groups 2–9 on days 0, 7, and 14 were 16.8±0.2, 16.9±0.2, and 16.5±0.2 g, respectively. Both WBC and RBC densities of mice treated with gemcitabine were significantly lower than those of the control ($p<0.05$); however, mice treated with β-lapachone and/or anti-EMMPRIN antibody were not significantly different ($p>0.05$) from control mice. Furthermore, the WBC and RBC

densities of mice treated with gemcitabine were not significantly different ($p>0.05$) from animals exposed to dual or triple combination therapies.

Discussion

It has been often perceived that tumor vascularity would evolve from avascularity to hypervascularity (*i.e.*, angiogenic switch). But this study demonstrated that it was a misperception by over-generalization; tumors evolve from avascularity to hypovascularity and then to hypervascularity, as shown in Fig. 2. In hypovascular tumors, the antiangiogenic effects of the anti-EMMPRIN antibody may reduce the efficiency of chemotherapy delivery when used in combination, producing an antagonistic effect, as demonstrated in this study. In a previous study, however, we showed a synergistic effect between the anti-EMMPRIN antibody and gemcitabine when the same mouse model (orthotopic MIA PaCa-2 tumor) was employed [19]. In that study, the initial tumor size was 238±38 mm^3, so the mean tumor K^{trans} value can be estimated to be 0.071±0.001 min^{-1} based on the data provided in Fig. 2c, which is about 60 % larger than that of tumors used in the current study. Therefore, for hypervascular tumors, the antiangiogenic effects of anti-EMMPRIN antibody may induce vascular normalization, thereby improving delivery of chemotherapy to tumors. We recently showed that the concentration of MR contrast agent (gadoteridol) in tumors at 40 min after injection increased about 150 % for only 3 days after the initiation of anti-EMMPRIN therapy when tumors were hypervascular (K^{trans} value, 0.058±13 min^{-1}), while both the K^{trans} and k_{ep} values of the tumors decreased about 40 % and 20 %, respectively, during the same time [25].

Therefore, it appears necessary to characterize tumor vascularity prior to therapy initiation. This may be the determining factor of whether addition of anti-EMMPRIN antibody to a given chemotherapeutic regimen will improve clinical outcome. About 85 % of primary pancreatic tumors and 60 % of liver metastases are known to be hypovascular [26, 27]. Fig. 5 illustrates how a vascular-guided personalized anti-EMMPRIN therapy could be applied in a clinical setting. The tumor biopsy specimen remaining after histological confirmation could be utilized to evaluate EMMPRIN expression on the cell membrane. Pancreatic cancers at diagnosis can be classified into three groups: resectable, non-resectable locally advanced, and metastatic cancers. For resectable pancreatic cancer (about 15 % of patients at diagnosis [28]), surgery would be performed first, followed by subsequent adjuvant therapy; combination therapy will be applied only for patients with EMMPRIN-positive tumors. For non-resectable locally advanced pancreatic cancer (about 40 % [29]), the primary tumor vascularity will be evaluated by DCE-MRI first, and combination therapy can be applied for patients with EMMPRIN-positive, hypervascular tumors. About 45 % of pancreatic cancer patients have metastases at diagnosis [30], most commonly in liver, peritoneum, and lung. DCE-MRI has been evaluated as a tool to assess tumor vascularity in lung and abdominal metastases using motion-correction techniques [31, 32]. If these metastases have different vascularity from the primary pancreatic tumor [26], therapy will be determined according to the vascularity of metastases to prevent further progress of them. One study showed that no patients had simultaneous hyper- and hypovascular metastatic tumors [26].

However, K^{trans} and k_{ep} values can be highly variable depending on the use of different imaging protocols and quantification methods [33]. Significant differences in quantitating the imaging pharmacokinetic parameters (K^{trans} and k_{ep}) were observed among commercially available computer software analyzing blood perfusion [34]. Therefore, there is an urgent need for standardization of DCE-MRI methodology for the clinical translation of vascular-guided personalized anti-EMMPRIN therapy.

To the best of our knowledge, these studies are the first to validate the efficacy of combination therapy with β-lapachone and gemcitabine in an orthotopic pancreatic cancer model *in vivo*. Although synergy between these two agents was expected, since β-lapachone can synergize with most DNA damaging agents, we noted only additive effects. β-Lapachone causes extensive DNA single-strand breaks [3] and thereby could synergize with the DNA damage created by gemcitabine. However, we used a dose of β-lapachone that was efficacious on its own. A lethal dose of β-lapachone leads to PARP1 hyperactivation *in vivo* [35], resulting in massive NAD+ and ATP losses that are likely to freeze cell metabolism and block/interfere with incorporation of nucleoside analogs, such as gemcitabine. Thus, synergy might have been achieved if the sub-lethal dose of β-lapachone had been used together with the lethal dose of gemcitabine. We are currently testing optimal timing and dosing of this combination to achieve nontoxic doses that together hyperactivate PARP1 and yield synergistic antitumor activities. Finally, we noted that β-lapachone caused significant reduction of glucose utilization in Mia PaCa-2 xenografts. We speculate that this reduction could be due to PARP1 hyperactivation-related NAD+/ATP losses. Effects of this drug, as well as other NQO1 bioactivatable drugs, on glucose utilization pathways are currently under investigation.

Conclusions

Antagonistic effects between anti-EMMPRIN antibody and two separate chemotherapeutic regimens were observed for hypovascular MIA PaCa-2 tumors. Thus, anti-EMMPRIN antibody may need to be considered only for patients with hypervascular tumors, when chemotherapy is used in combination.

Acknowledgments

Authors thank Dr. Lingling Guo for aid in surgically inserting mouse vascular ports and Dr. Eben L. Rosenthal for help in initial study design and consultation. The authors also thank Lee Whitworth and Dr. Jason M. Warram for assistance in growing MIA PaCa-2 cells, animal monitoring, imaging, and drug dosing. We thank Dr. Brenda Yamamoto for analyses of blood cells. This study was supported by a Research Initiative Pilot Award from the Department of Radiology at UAB and NIH grants 2P30CA013148, R01CA142637, P50CA101955, and R01CA102792-13.

References

1. Burris HA III, Moore MJ, Andersen J, et al. Improvements in survival and clinical benefit with gemcitabine as first-line therapy for patients with advanced pancreas cancer: a randomized trial. J Clin Oncol. 1997; 15:2403–2413. [PubMed: 9196156]
2. Bentle MS, Reinicke KE, Bey EA, Spitz DR, Boothman DA. Calcium-dependent modulation of poly(ADP-ribose) polymerase-1 alters cellular metabolism and DNA repair. J Biol Chem. 2006; 281:33684–33696. [PubMed: 16920718]

3. Bey EA, Bentle MS, Reinicke KE, et al. An NQO1- and PARP-1-mediated cell death pathway induced in non-small-cell lung cancer cells by beta-lapachone. Proc Natl Acad Sci U S A. 2007; 104:11832–11837. [PubMed: 17609380]
4. Tagliarino C, Pink JJ, Dubyak GR, Nieminen AL, Boothman DA. Calcium is a key signaling molecule in beta-lapachone-mediated cell death. J Biol Chem. 2001; 276:19150–19159. [PubMed: 11279125]
5. Boothman DA, Pardee AB. Inhibition of radiation-induced neoplastic transformation by beta-lapachone. Proc Natl Acad Sci U S A. 1989; 86:4963–4967. [PubMed: 2740334]
6. Riethdorf S, Reimers N, Assmann V, et al. High incidence of EMMPRIN expression in human tumors. Int J Cancer. 2006; 119:1800–1810. [PubMed: 16721788]
7. Caudroy S, Polette M, Nawrocki-Raby B, et al. EMMPRIN-mediated MMP regulation in tumor and endothelial cells. Clin Exp Metastasis. 2002; 19:697–702. [PubMed: 12553375]
8. Braundmeier AG, Fazleabas AT, Lessey BA, Guo H, Toole BP, Nowak RA. Extracellular matrix metalloproteinase inducer regulates metalloproteinases in human uterine endometrium. J Clin Endocrinol Metab. 2006; 91:2358–2365. [PubMed: 16522689]
9. Dalberg K, Eriksson E, Enberg U, Kjellman M, Backdahl M. Gelatinase A, membrane type 1 matrix metalloproteinase, and extracellular matrix metalloproteinase inducer mRNA expression: correlation with invasive growth of breast cancer. World J Surg. 2000; 24:334–340. [PubMed: 10658069]
10. Ellenrieder V, Alber B, Lacher U, et al. Role of MT-MMPs and MMP-2 in pancreatic cancer progression. Int J Cancer. 2000; 85:14–20. [PubMed: 10585576]
11. Bougatef F, Quemener C, Kellouche S, et al. EMMPRIN promotes angiogenesis through hypoxia-inducible factor-2alpha-mediated regulation of soluble VEGF isoforms and their receptor VEGFR-2. Blood. 2009; 114:5547–5556. [PubMed: 19837976]
12. Jain RK. Normalizing tumor vasculature with anti-angiogenic therapy: a new paradigm for combination therapy. Nat Med. 2001; 7:987–989. [PubMed: 11533692]
13. Kim H, Folks KD, Guo L, et al. Early therapy evaluation of combined cetuximab and irinotecan in orthotopic pancreatic tumor xenografts by dynamic contrast-enhanced magnetic resonance imaging. Mol Imaging. 2011; 10:153–167. [PubMed: 21496446]
14. Dandekar M, Tseng JR, Gambhir SS. Reproducibility of 18F-FDG microPET studies in mouse tumor xenografts. J Nucl Med. 2007; 48:602–607. [PubMed: 17401098]
15. Kroep JR, Van Groeningen CJ, Cuesta MA, et al. Positron emission tomography using 2-deoxy-2-[18F]-fluoro-D-glucose for response monitoring in locally advanced gastroesophageal cancer; a comparison of different analytical methods. Mol Imaging Biol. 2003; 5:337–346. [PubMed: 14630513]
16. Kelloff GJ, Hoffman JM, Johnson B, et al. Progress and promise of FDG-PET imaging for cancer patient management and oncologic drug development. Clin Cancer Res. 2005; 11:2785–2808. [PubMed: 15837727]
17. Kim H, Folks KD, Guo L, et al. DCE-MRI detects early vascular response in breast tumor xenografts following anti-DR5 therapy. Mol Imaging Biol. 2011; 13:94–103. [PubMed: 20383593]
18. Zetter BR. Angiogenesis and tumor metastasis. Annu Rev Med. 1998; 49:407–424. [PubMed: 9509272]
19. Shah N, Zhai G, Knowles JA, et al. (18)F-FDG PET/CT imaging detects therapy efficacy of anti-EMMPRIN antibody and gemcitabine in orthotopic pancreatic tumor xenografts. Mol Imaging Biol. 2012; 14:237–244. MIB : the official publication of the Academy of Molecular Imaging. [PubMed: 21494920]
20. Kim H, Zhai G, Liu Z, et al. Extracelluar matrix metalloproteinase as a novel target for pancreatic cancer therapy. Anti-Cancer Drugs. 2011; 22:864–874. [PubMed: 21730821]
21. Kim H, Morgan DE, Zeng H, et al. Breast tumor xenografts: diffusion-weighted MR imaging to assess early therapy with novel apoptosis-inducing anti-DR5 antibody. Radiology. 2008; 248:844–851. [PubMed: 18710978]
22. Neter, J.; Kutner, MH.; Nachtsheim, JC.; Wasserman, W. Applied linear statistical models. The McGraw-Hill Companies, Inc; Columbus: 1996.

23. Hertzog C, Rovine M. Repeated-measures analysis of variance in developmental research: selected issues. Child Dev. 1985; 56:787–809. [PubMed: 4042744]
24. Rodgers JL, Nicewander WA. Thirteen ways to look at the correlation coefficient. Am Stat. 1988; 42:59–66.
25. Kim H, Zhai G, Samuel SL, et al. Dual combination therapy targeting DR5 and EMMPRIN in pancreatic adenocarcinoma. Mol Cancer Ther. 2012; 11:405–415. [PubMed: 22203731]
26. Danet IM, Semelka RC, Nagase LL, Woosely JT, Leonardou P, Armao D. Liver metastases from pancreatic adenocarcinoma: MR imaging characteristics. J Magn Reson Imaging. 2003; 18:181–188. JMRI. [PubMed: 12884330]
27. Sofuni A, Iijima H, Moriyasu F, et al. Differential diagnosis of pancreatic tumors using ultrasound contrast imaging. J Gastroenterol. 2005; 40:518–525. [PubMed: 15942718]
28. Andersson R, Vagianos CE, Williamson RC. Preoperative staging and evaluation of resectability in pancreatic ductal adenocarcinoma. HPB. 2004; 6:5–12. The Official Journal of the International Hepato Pancreato Biliary Association. [PubMed: 18333037]
29. Willett CG, Czito BG, Bendell JC, Ryan DP. Locally advanced pancreatic cancer. J Clin Oncol. 2005; 23:4538–4544. Official Journal of the American Society of Clinical Oncology. [PubMed: 16002845]
30. Cardenes HR, Chiorean EG, Dewitt J, Schmidt M, Loehrer P. Locally advanced pancreatic cancer: current therapeutic approach. Oncologist. 2006; 11:612–623. [PubMed: 16794240]
31. Chang YC, Yu CJ, Chen CM, et al. Dynamic contrast-enhanced MRI in advanced nonsmall-cell lung cancer patients treated with first-line bevacizumab, gemcitabine, and cisplatin. J Magn Reson Imaging. 2012; 36:387–396. JMRI. [PubMed: 22517425]
32. Coenegrachts K, Bols A, Haspeslagh M, Rigauts H. Prediction and monitoring of treatment effect using T1-weighted dynamic contrast-enhanced magnetic resonance imaging in colorectal liver metastases: potential of whole tumour ROI and selective ROI analysis. Eur J Radiol. 2012; 81:3870–3876. [PubMed: 22944331]
33. Zwick S, Brix G, Tofts PS, et al. Simulation-based comparison of two approaches frequently used for dynamic contrast-enhanced MRI. Eur Radiol. 2010; 20:432–442. [PubMed: 19727758]
34. Heye T, Davenport MS, Horvath JJ, et al. Reproducibility of dynamic contrast-enhanced MR imaging. Part I. Perfusion characteristics in the female pelvis by using multiple computer-aided diagnosis perfusion analysis solutions. Radiology. 2013; 266:801–811. [PubMed: 23220897]
35. Huang X, Dong Y, Bey EA, et al. An NQO1 substrate with potent antitumor activity that selectively kills by PARP1-induced programmed necrosis. Cancer Res. 2012; 72:3038–3047. [PubMed: 22532167]

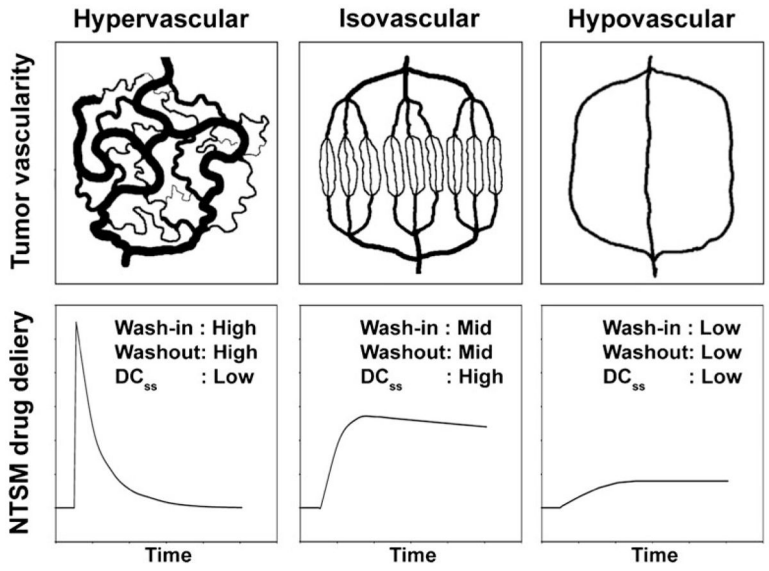

Fig. 1.

Theoretical illustration of the delivery of a non-targeting small-molecule (NTSM) drug over time to tumors with varying vascularity. DC_{ss} stands for NTSM drug concentration at steady-state in the tumor.

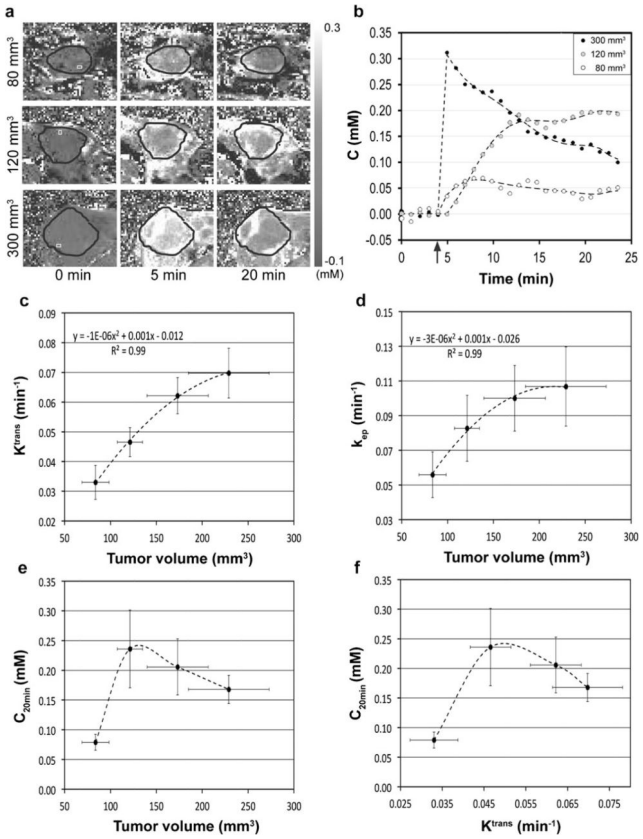

Fig. 2.

MIA PaCa-2 tumor vascularity correlated with tumor size. **a** MR contrast agent (*i.e.*, gadoteridol) concentration in three representative mice bearing different-sized MIA PaCa-2 pancreatic tumors at t=0 (baseline), 5, and 20 min after injection. Tumor region is indicated with a *black circle* in each sub-figure. **b** Contrast-enhancement curves averaged in the ROIs indicated with *white squares* shown in Fig. 2a, while the time point of gadoteridol injection is indicated with a *black arrow*. **c** Mean K^{trans} values *versus* mean tumor volumes. **d** Mean k_{ep} values *versus* mean tumor volumes. **e** Mean C_{20min} values *versus* mean tumor volumes. **f** Mean C_{20min} values *versus* mean K^{trans} values.

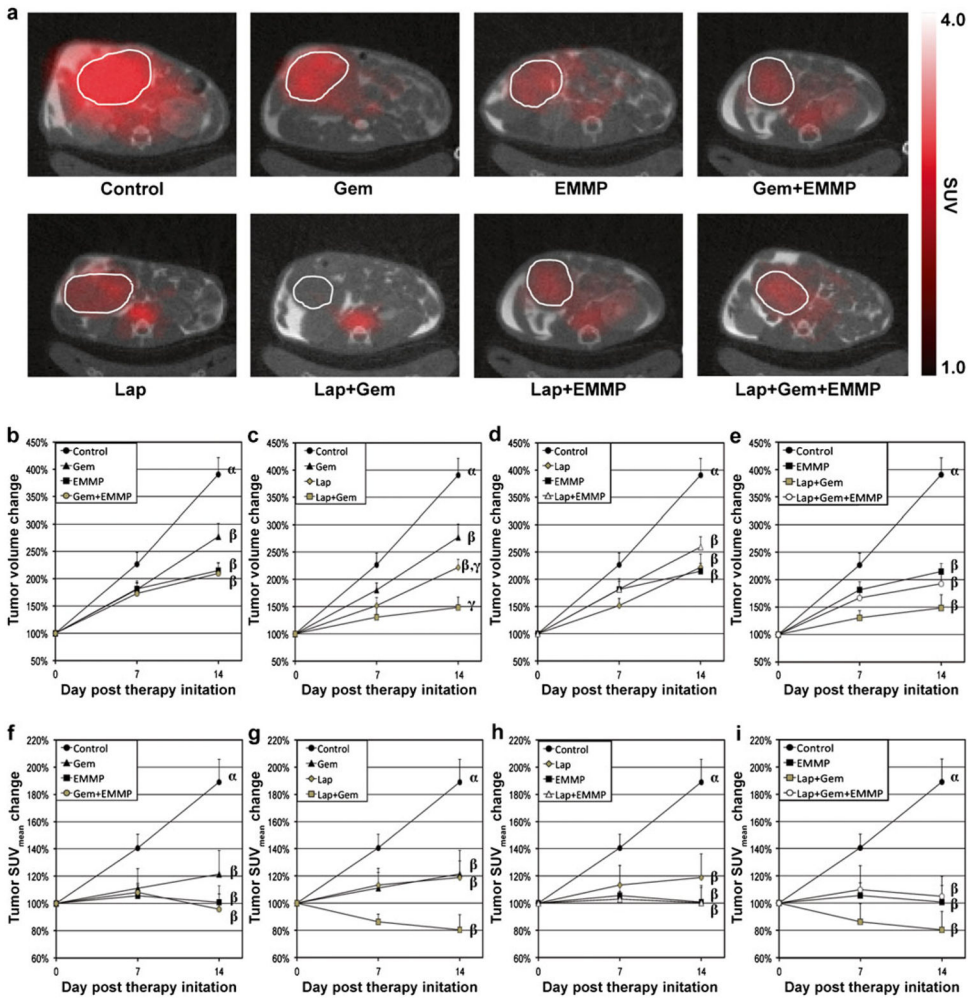

Fig. 3.

In vivo 2-Deoxy-2-[^{18}F]fluoro-D-glucose-positron emission tomography/computed tomography (FDG-PET/CT) image analyses *in vivo*. **a** Representative ^{18}F-FDG-PET, contrast-enhanced CT (CE-CT), and PET/CT fused images of mice from groups 2–9 at 2 weeks after therapy initiation. Tumor location is indicated with a *white circle* in each sub-figure. The same color scale was applied to all PET images. **b** Tumor volume and **f** SUV_{mean} changes of four groups untreated (control) or treated with gemcitabine, anti-EMMPRIN antibody, and combination, respectively. **c** Tumor volume and **g** SUV_{mean} changes of four groups untreated (control) or treated with β-lapachone, gemcitabine, and combination, respectively. **d** Tumor volume and **h** SUV_{mean} changes of four groups untreated (control) or treated with β-lapachone, anti-EMMPRIN antibody, and combination, respectively. **e** Tumor volume and **i** SUV_{mean} changes in mice untreated (control) or treated with anti-EMMPRIN antibody, combined therapy with β-lapachone and gemcitabine, or the triple combination therapy, respectively. Statistical differences among groups are represented with different *Greek letters* (*Lap*: β-lapachone; *EMMP*: anti-EMMPRIN antibody; *Gem*: gemcitabine).

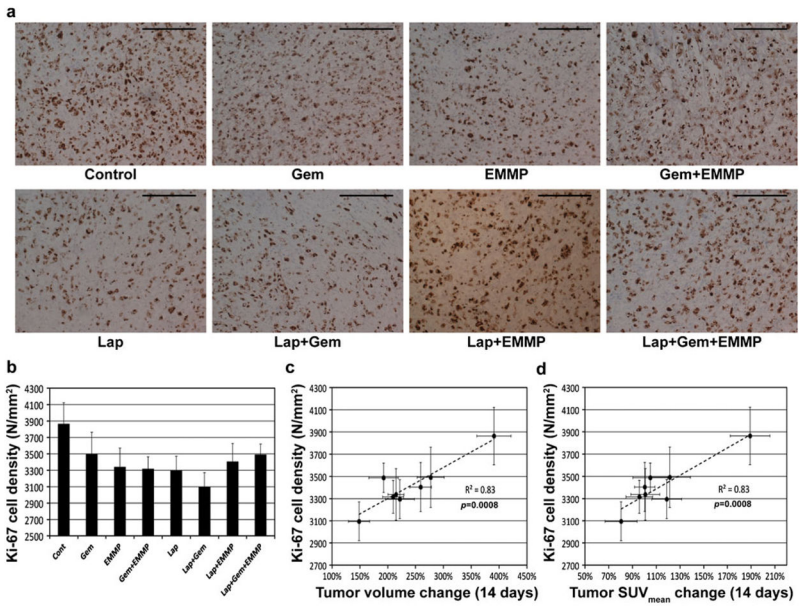

Fig. 4.

Histological analyses of tumor responses. **a** Representative microphotographs of tumor tissues following various therapies (*Gem*: gemcitabine; *EMMP*: anti-EMMPRIN antibody; *Lap*: β-lapachone), showing Ki-67 expressing cells (*dark brown*). The length of each scale *bar* is 0.1 mm. **b** Ki-67 cell densities of tumor tissues from groups 2–9. **c**, **d** Correlations between Ki-67 cell densities and **c** tumor volume changes or **d** tumor SUV_{mean} changes for 14 days after therapy initiation.

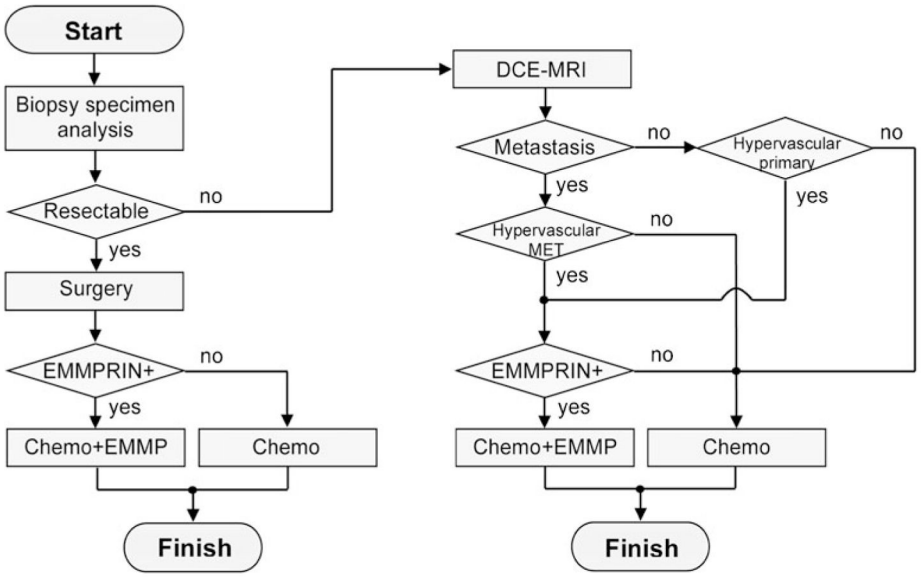

Fig. 5.

Flow chart showing a proposed therapeutic strategy based on cancer stage, EMMPRIN expression, and tumor vascularity (*Chemo*: chemotherapy; *EMMP*: anti-EMMPRIN therapy; *MET*: metastasis).